

A Redox-Regulated, Heterodimeric NADH:cinnamate Reductase in *Vibrio ruber*

Yulia V. Bertsova^{1,a}, Marina V. Serebryakova^{1,b}, Victor A. Anashkin^{1,c},
Alexander A. Baykov^{1,d}, and Alexander V. Bogachev^{1,e*}

¹Belozersky Institute of Physico-Chemical Biology, Lomonosov Moscow State University, 119234 Moscow, Russia

^ae-mail: bertsova@belozersky.msu.ru

^be-mail: mserebr@mail.ru

^ce-mail: victor_anashkin@belozersky.msu.ru

^de-mail: baykov@belozersky.msu.ru

^ee-mail: bogachev@belozersky.msu.ru

Received June 24, 2023

Revised October 9, 2023

Accepted October 10, 2023

Abstract—Genes of putative reductases of α,β -unsaturated carboxylic acids are abundant among anaerobic and facultatively anaerobic microorganisms, yet substrate specificity has been experimentally verified for few encoded proteins. Here, we co-produced in *Escherichia coli* a heterodimeric protein of the facultatively anaerobic marine bacterium *Vibrio ruber* (GenBank SJN56019 and SJN56021; annotated as NADPH azoreductase and urocanate reductase, respectively) with *Vibrio cholerae* flavin transferase. The isolated protein (named Crd) consists of the *sjn56021*-encoded subunit CrdB (*NADH:flavin*, *FAD binding 2*, and *FMN bind* domains) and an additional subunit CrdA (SJN56019, a single *NADH:flavin* domain) that interact via their *NADH:flavin* domains (AlphaFold2 prediction). Each domain contains a flavin group (three FMNs and one FAD in total), one of the FMN groups being linked covalently by the flavin transferase. Crd readily reduces cinnamate, *p*-coumarate, caffeate, and ferulate under anaerobic conditions with NADH or methyl viologen as the electron donor, is moderately active against acrylate and practically inactive against urocanate and fumarate. Cinnamates induced Crd synthesis in *V. ruber* cells grown aerobically or anaerobically. The Crd-catalyzed reduction started by NADH demonstrated a time lag of several minutes, suggesting a redox regulation of the enzyme activity. The oxidized enzyme is inactive, which apparently prevents production of reactive oxygen species under aerobic conditions. Our findings identify Crd as a regulated NADH-dependent cinnamate reductase, apparently protecting *V. ruber* from (hydroxy)cinnamate poisoning.

DOI: 10.1134/S0006297924020056

Keywords: anaerobic respiration, cinnamic acid, caffeic acid, enzyme regulation, reactive oxygen species, rhizosphere, *Vibrio*

INTRODUCTION

NADH:2-enoate reductases (EC 1.3.1.31) capable of reducing α,β -unsaturated carboxylic acids, such as fumaric, cinnamic, and acrylic acids, are abundant among anaerobic and facultatively anaerobic micro-

organisms [1-4]. All known 2-enoate reductases are formed by single polypeptides but are divided into two non-homologous groups according to their variable domain composition. The three-domain reductases invariably contain a *FAD binding 2* domain (Pfam ID: PF00890), which has a noncovalently bound FAD

Abbreviations: aCrd, non-flavinylated Crd protein containing only non-covalently bound flavins; fCrd, flavinylated Crd protein; *FMN, covalently bound FMN residue; MS, mass spectrometry, MV, methyl viologen, *m/z*, mass-to-charge ratio; MD, molecular dynamics; ROS, reactive oxygen species.

* To whom correspondence should be addressed.

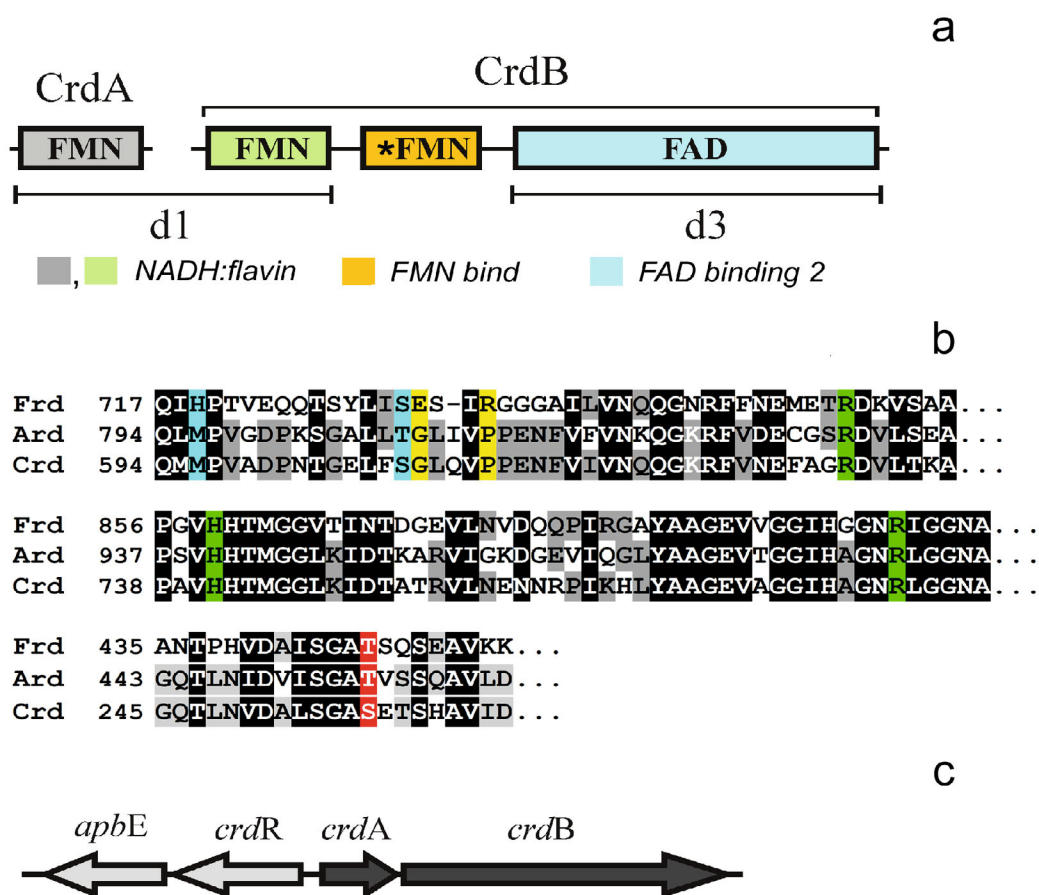


Fig. 1. Bioinformatic description of *V. ruber* Crd and its genes. **a)** The domain composition of the polypeptides CrdA and CrdB forming the Crd heterodimer. The *NADH:flavin*, *FMN bind*, and *FAD binding 2* domains (residues 1-180, 190-275, and 280-800, respectively) are indicated by different colors. Domain names are taken from the Pfam database. Putative redox-active prosthetic groups are shown inside the boxes. The asterisk denotes the covalently bound flavin. The truncated versions of Crd obtained in this study are denoted as d1 and d3. **b)** Sequence alignment of the fumarate reductase from *K. pneumoniae* (Frd, UniProt accession number B5XRB0), acrylate reductase from *V. harveyi* (Ard, P0DW92), and CrdB protein from *V. ruber* (GenBank accession number SJN56021) with Clustal [42]. The three parts of the alignment shown contain the amino acid residues involved in fumarate C1- and C4-carboxylate binding in Frd (marked in blue and green, respectively), the proton transfer to fumarate (marked in yellow) in Frd, and covalent bonding with FMN in all shown proteins (marked in red). **c)** The arrangement of the *crd*-associated genes in a *V. ruber* chromosome. ApbE, putative FAD:protein FMN transferase; CrdR, putative transcription regulator.

prosthetic group and is the place of carbonic acid reduction. NADH is oxidized in *OYE-like* (PF00724) or *FAD binding 6* (PF00970) domain having noncovalently bound FMN or FAD, respectively [2, 3]. The third domain (commonly *FMN bind*; PF04205) mediates electron transfer between the above domains via a flavin group (FMN) which is covalently bound by a phosphoester bond [4-6].

Many bacteria of the class Clostridia have a two-domain 2-enoate reductase [1, 7], formed by *OYE-like* and *Pyr redox 2* (PF07992) domains. The reductases of this group contain a [4Fe-4S] cluster and noncovalently bound FAD and FMN in a 1:1:1 ratio as prosthetic groups [8, 9]. In saccharolytic clostridia, two-domain 2-enoate reductases convert a broad range of 2-enoates, whereas the enzymes from proteolytic clostridia are highly specific and convert only cinnamate and its

derivatives [10, 11]. All known 2-enoate reductases do not appear to be regulated at activity level, except by substrates and products.

The genome of the red facultatively anaerobic marine bacterium *Vibrio ruber* [12] encodes a polypeptide formed by 806 amino acid residues and annotated as urocanate reductase in GenBank (SJN56021) and in UniProt (A0A1R4LHH9). This polypeptide, which we designate as CrdB, based on the substrate specificity of its containing enzyme (see below), encompasses the abovementioned *FAD binding 2* and *FMN bind* domains (Fig. 1a). Five putative substrate-binding residues, identified in the *FAD binding 2* domains of CrdB and acrylate reductase of *Vibrio harveyi* by comparison with fumarate reductase [4, 13, 14] (Fig. 1b), are identical or very similar, suggesting that CrdB is an acrylate reductase. The *FMN bind* domain of CrdB, like its counter-

parts in known 2-enoate reductases, contains the motif DALSGAS₂₅₇ recognized by flavin transferase for covalent FMN attachment to the serine residue [15]. Noteworthy, the gene *apbE* encoding the flavin transferase (GenBank ID: SJN56016) locates nearby to *crdB* in one of the two *V. ruber* chromosomes (Fig. 1c). Altogether, these characteristics of CrdB classify it as a three-domain 2-enoate reductase with a likely acrylate reductase activity.

However, the CrdB protein differs from established three-domain 2-enoate reductases by its third, *NADH:flavin* domain (PF03358) replacing the *NADH*-oxidizing domains *OYE-like* or *FAD binding 6* (Fig. 1a). Furthermore, the *crd*-operon of *V. ruber* contains, upstream of the *crdB* gene, the gene *crdA* encoding a protein (SJN56019) (Fig. 1c) formed by a single *NADH:flavin* domain that is homologous (51% identity, 65% similarity) to the similar domain of CrdB. As *NADH:flavin* domains can dimerize [16], this observation raised an intriguing possibility of Crd functioning as a CrdA/CrdB heterodimer.

Keeping in mind the difficulty in the theoretical prediction of the enzymatic activities and substrate specificities of *NADH*:2-enoate reductases, we have produced the *V. ruber* Crd protein in *Escherichia coli* cells and characterized the isolated protein. The data reported below identify Crd as a regulated *NADH*-dependent reductase active against cinnamic acid and its various derivatives.

MATERIALS AND METHODS

Bacterial strains and growth conditions. *V. ruber* DSM 16370 was obtained from the Leibniz Institute collection of microorganisms and cell cultures (DSMZ). The cells were grown aerobically or anaerobically at 28°C in a mineral medium containing 20 g/liter NaCl, 0.75 g/liter KCl, 1.2 g/liter MgSO₄·7(H₂O), 0.5 g/liter NH₄Cl, 0.5 mM Na₂HPO₄, 2 g/liter sucrose, 0.5 g/liter yeast extract, and 50 mM Tris-HCl (pH 8.0). When required, the medium was supplemented with 2–10 mM acrylate, cinnamate, *p*-coumarate, caffeate, or ferulate. Cleared cell lysate was prepared as described elsewhere [17] and assayed for MV:cinnamate reductase activity. *E. coli* cells were grown at 37°C in LB. Where indicated, the LB medium was supplemented with 20 µg/ml chloramphenicol and (or) 100 µg/ml ampicillin.

Construction of expression vectors. The expression vector for the CrdAB protein with C-terminal 6×His-tagged CrdB was constructed by amplifying the *crd*-operon from the genomic *V. ruber* DNA. A high-fidelity Tarsus polymerase (Evrogen, Russia) and the primers V_ruber_DIR/V_ruber_REV were used (primer sequences are listed in Table S1 in the Online Resource 1). The resulting 3276-bp fragment was cloned

into the pBAD-TOPO vector (Invitrogen, USA), yielding the pTB_CRD4 plasmid. The plasmid was transformed into *E. coli*/pΔhis3 [18] or BL21 strains.

The expression vector for the d1 fragment (full-size CrdA and residues 1–184 of CrdB) was constructed by amplifying the corresponding DNA fragment of the *crd*-operon by PCR with a Tarsus PCR kit and the primers V_ruber_DIR/VR_P1R using *V. ruber* genomic DNA as the template. The resulting 1401-bp fragment was cloned into the pBAD-TOPO vector, yielding the pTB_d1CRD17 plasmid. To construct an expression vector for the d3 fragment (residues 281–806) of CrdB, the 1688-bp fragment was amplified by PCR with the VR_3P2_NdeD/Xho_rhod_rev primer pair and the pTB_CRD4 plasmid as the template. The amplified fragment was cloned into the pSCodon vector (Delphi Genetics, Belgium) using the *NdeI/XhoI* sites, resulting in the plasmid pSC_d3CRD2. The pTB_d1CRD17 and pSC_d3CRD2 plasmids were transformed into *E. coli* BL21 strain.

Crd production. The 6×His-tagged Crd proteins with or without covalently bound FMN (fCrd and aCrd, respectively) and the d1 and d3 fragments of Crd were produced in *E. coli* BL21 or pΔhis3 cells and purified using metal chelate chromatography as described previously [5]. The extinction coefficients $\epsilon_{450\text{nm}}$ for fCrd, aCrd, d1 fragment, and d3 fragment determined after SDS treatment [4] were 42, 31, 22, and 11 mM⁻¹ cm⁻¹, respectively.

Analysis of flavins. Non-covalently bound flavins were extracted from Crd preparations by trifluoroacetic acid (TFA) and separated by HPLC [5]. SDS-PAGE was performed using 12.5% (w/v) polyacrylamide gels [19]. The gels were stained for protein with PageBlue™ solution (Fermentas, Lithuania). Covalently bound flavins were detected by scanning unstained gels with a Typhoon™ FLA 9500 laser scanner (GE Healthcare, USA) with excitation at 473 nm and the detection of emission using the SYBR Green II protocol according to the manufacturer's recommendations.

For mass-spectral measurements, gel pieces of approximately 2 mm³ were excised from the protein bands of the Coomassie-stained gel and destained by incubating in two 0.1-ml volumes of 40% (by volume) acetonitrile solution containing 20 mM NH₄HCO₃, pH 7.5, dehydrated with 0.2 ml of 100% acetonitrile and rehydrated with 5 µl of the digestion solution containing 15 µg/ml sequencing-grade trypsin (Promega, USA) in 20 mM aqueous solution of NH₄HCO₃, pH 7.5. Digestion was carried out at 37°C for 1 h. The resulting peptides were extracted with 5 µl 30% acetonitrile solution containing 0.5% TFA. A 1-µl aliquot of the in-gel tryptic digest extract was mixed with 0.5 µl of 2,5-dihydroxybenzoic acid solution (40 mg/ml) in 30% acetonitrile containing 0.5% TFA and left to dry on a stainless-steel target plate. MALDI-TOF MS analysis

was performed on an UltrafleXtreme MALDI-TOF-TOF mass spectrometer (Bruker Daltonik, Germany). The MH^+ molecular ions were measured in a reflector mode; the accuracy of monoisotopic mass peak measurement was within 30 ppm. Spectra of fragmentation were obtained in a LIFT mode; the accuracy of daughter ion measurement was within 1 Da. Mass-spectra were processed with the FlexAnalysis 3.2 software (Bruker Daltonik). Protein identification was carried out by MS+MS/MS ion search, using Mascot software version 2.3.02 (Matrix Science, USA), through the Home NCBI Protein Database. One each of missed cleavage, Met oxidation, Cys-propionamide, and Ser(Thr)-FMN were permitted. Protein scores greater than 94 were considered significant ($p < 0.05$).

Enzymatic activities. NADH- and methyl viologen (MV)-supported activities of Crd preparations were determined at 25°C by following NADH or MV oxidation spectrophotometrically at 340 or 606 nm, respectively, with a Hitachi-557 spectrophotometer [3]. The assay medium contained 1 mM MV, 0.03–1 mM electron acceptor, and 100 mM Tris-HCl (pH 8.0) or 120 μ M NADH, 0.05–1 mM electron acceptor, 10 mM glucose, 5 U/ml glucose oxidase, 5 U/ml catalase, and 100 mM Mes-KOH (pH 6.5) in a completely filled and sealed 3.2-ml cuvette. MV was pre-reduced with sodium dithionite until the absorbance at 606 nm of approximately 1.5 was obtained, which corresponds to the formation of \sim 100 μ M reduced MV. Unless otherwise noted, Crd or its variant was preincubated with NADH or MV for 5 min before the reaction was started by adding an electron acceptor. The NADH-supported reaction was also measured under aerobic conditions without glucose oxidase and catalase. Crd activities were calculated using the experimentally verified NADH:acceptor and MV:acceptor stoichiometries of 1 : 1 and 2 : 1, respectively.

The assay medium for measuring FMN₂:cinnamate reductase activity contained 100 μ M FMN, 1 mM cinnamate, and 100 mM Tris-HCl (pH 8.0). FMN was pre-reduced with sodium dithionite until the absorbance at 450 nm decreased to a value of \sim 0.3, which corresponds to formation of \sim 70 μ M reduced FMN. FMN₂ oxidation was followed spectrophotometrically at 450 nm.

Phenylpropionate dehydrogenase activity was assayed by measuring the reduction of 2,6-dichlorophenolindophenol (DCPIP, $\epsilon_{600} = 22 \text{ mM}^{-1} \text{ cm}^{-1}$) at 600 nm [20]. The assay mixture contained 2 mM Tris-phenylpropionate, 2 mM phenazine methosulphate, 25 μ M DCPIP, and 100 mM Mes-KOH (pH 6.5).

The Michaelis–Menten parameters of MV-supported acrylate reduction by Crd were estimated from duplicate measurements of the initial rates of MV oxidation using 0.03–10 mM acrylate and 40 nM Crd concentrations. For other electron acceptors, rates were obtained from the integral kinetics of their reduction

until its completion, as monitored by absorbance at 606 nm. Rates were estimated at 100 time points along the progress curve as the slopes of the tangents ($-d[MV]/dt$) using MATLAB (The MathWorks, Inc.). The residual electron acceptor concentration was calculated at each point from A_{606} using the MV:acceptor stoichiometry of 2 : 1 and assuming that the limiting value of A_{606} corresponds to 100% conversion of the electron acceptor. The Michaelis–Menten equation was fitted to the rate data using non-linear regression analysis.

Identification of the product of cinnamate reduction. Cinnamate reduction was performed in 3.2 ml of the medium containing 100 μ M cinnamate, 10 mM sodium dithionite, 50 μ M MV, and 100 mM Tris-HCl (pH 8.0). The reaction was initiated by adding 0.5 μ M Crd and terminated after 30 min by adding 5% (vol/vol) HClO₄. In the control experiment, HClO₄ was added before Crd. Precipitated protein was removed by centrifugation, and the substrate and products were extracted from the samples with diethyl ether (2 \times 1.5 ml). The ether was evaporated under a stream of air, and the residue was dissolved in 1 ml of 25 mM potassium phosphate (pH 6.5) (medium A). The samples were separated by HPLC on a ProntoSil-120-5-C18 AQ column using a Milichrom A-02 chromatograph (both from Econova, Russia). The column was pre-equilibrated with medium A and eluted with a linear gradient from 0% to 10% methanol in medium A at a flow rate of 0.2 ml/min with UV detection at 210 and 258 nm.

Quantitative reverse transcription polymerase chain reaction (RT-qPCR). RNA extraction from *V. ruber* cells and cDNA synthesis were performed as described previously [17]. RT-qPCR assays were performed with qPCRmix-HS SYBR kit (Evrogen), using the cDNA preparations as templates and VR_69U19/VR_273L20 as primer pair for *crdB*. 16S rRNA was used for data normalization (the primer pair 16s FW/16s RV). Serial dilutions of *V. ruber* genomic DNA, which contains the genes for CrdB and 16S rRNA in a 1 : 8 ratio, were used for calibration.

Bioinformatics. The three-dimensional structure of flavin-deficient Crd was predicted from the amino acid sequences of CrdA and CrdB using AlphaFold2 (version 2.2.0) [21] through the ColabFold advanced notebook [22]. Multimer model prediction was performed using default parameter settings. The Ramachandran plot indicated that 96.7% residues have favorable dihedral angles in the modelled structure.

Ligands (flavins, NADH, cinnamate) were docked in sequence into the obtained Crd structure using AutoDock Vina [23] in the following sequence: *FMN, FAD, FMN_B, FMN_A, NADH, cinnamate. Space cells ranging from 12 \times 12 \times 12 to 30 \times 30 \times 30 Å³ were selected for docking in the appropriate regions of the protein based

on the known structures of homologous proteins. Each docking experiment was performed in triplicate. The derived Crd structure containing one FAD and three FMN groups was finally equilibrated by molecular dynamics (MD) simulations for 150 ns with AMBER 22 package [24] (<https://ambermd.org/>). Details of the simulation are found in Electronic Supplementary Materials (Fig. S4 legend in the Online Resource 1).

RESULTS

Production and characterization of *V. ruber* Crd.

The CrdAB operon of *V. ruber* genomic DNA was amplified and cloned into an expression vector that added a 6×His tag at the C-terminus of CrdB. The *FMN bind* domain of CrdB harbors the sequence DALSGAS₂₅₇, similar to the flavinylation motif Dxx(s/t)gA(T/S) recognized by flavin transferase for covalent attachment of FMN via a threonine or serine hydroxyl [15]. To test whether the predicted flavinylation really occurs, the *crd*-operon genes were expressed in *E. coli* cells in the presence or absence of the auxiliary pHis3 plasmid [18] that encodes the flavin transferase ApbE capable of flavinyllating *FMN bind* domains in various proteins [15]. The recombinant fCrd and aCrd proteins produced in the ApbE-containing and ApbE-lacking cells, respectively, were isolated by metal affinity chromatography. The final protein preparations were of intense yellow color, and their visible spectra (Fig. 2a) were characteristic of flavoproteins.

SDS-PAGE of both Crd preparations revealed one major and three-four minor protein bands (Fig. 2b, left image). Bands 1 and 3 were identified by the MALDI-MS analysis after trypsin digestion as *V. ruber* CrdB (sequence coverage of 79%) and CrdA (sequence coverage of 95%), respectively. Band 2 belonged to *E. coli* peptidyl-prolyl *cis-trans* isomerase SlyD, which exhibits high intrinsic affinity to Ni-agarose and is a common contamination of the 6×His-tagged proteins isolated from *E. coli* [25]. Band 1 derived from fCrd fluoresced when illuminated at 473 nm, indicating covalently bound flavin (Fig. 2b, right image). No bound flavin was detected by this method in aCrd. These findings provide convincing evidence for ApbE-mediated covalent flavinylation of CrdB. It should be noted that the non-covalently bound flavins, evidently present in both Crd preparations (Fig. 2a) are removed from the proteins during SDS-PAGE.

The CrdB flavinylation site was identified by MALDI-MS and MS/MS after trypsinolysis. The peptide I₂₄₂IEGQTLNVDALSGASETSHAVIDGVAK₂₆₉ containing the underlined flavinylation motif should have demonstrated the monoisotopic MH⁺ masses of 2795.3 and 3233.5 in the non-flavinyllated and flavinyllated forms, respectively. Both predicted signals were indeed

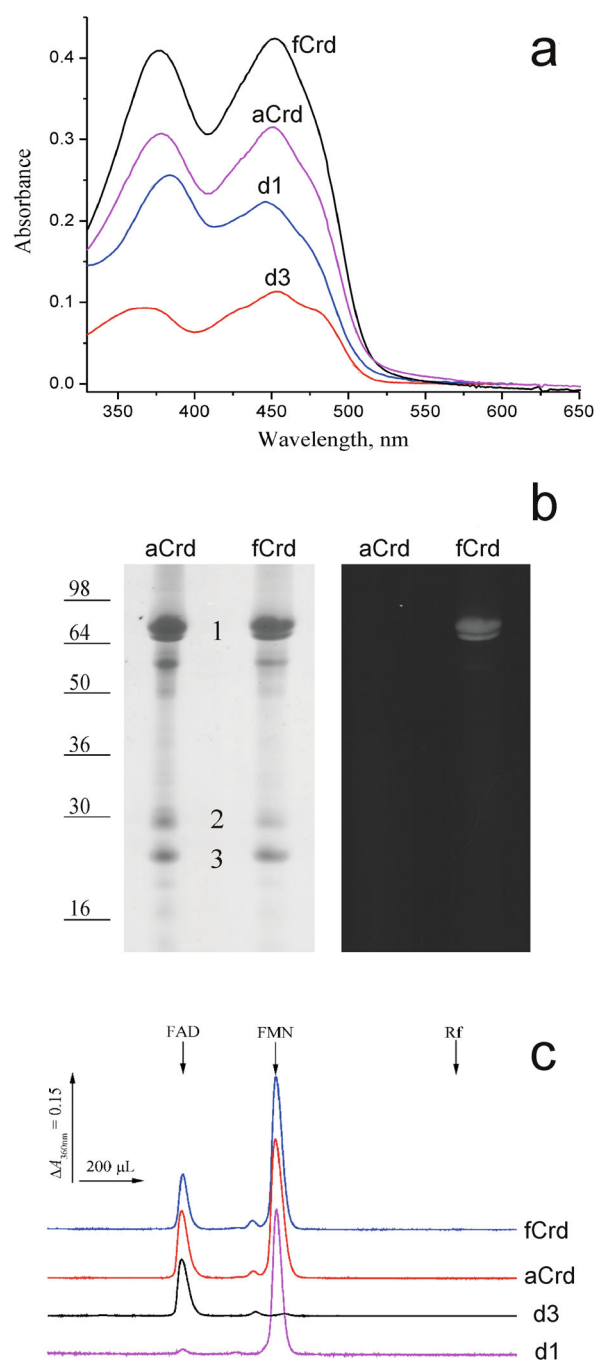


Fig. 2. Characterization of the Crd preparations. a) Electronic absorption spectra of the full-length and truncated (d1 and d2) Crd preparations at 10 μ M concentrations. Full-length Crd was produced in ApbE-containing or ApbE-lacking *E. coli* cells (fCrd and aCrd, respectively). b) SDS-PAGE of fCrd and aCrd. The gel was stained with Coomassie Blue (left image) or scanned under illumination at 473 nm without staining (right image). The protein load was 5 μ g per lane. Bars with numbers on the left side denote the positions and molecular masses of marker proteins. The protein bands identified by MALDI-MS analysis are marked by numbers. c) HPLC separation of non-covalently bound flavins in Crd and its truncated variants. The retention volumes for authentic FAD, FMN, and riboflavin (Rf) are indicated by arrows.

observed on the mass-spectrum of the tryptic digest of fCrdB. The presence of the former signal may reflect either incomplete modification or partial loss of the flavin group during SDS-PAGE and trypsin proteolysis. No other candidates for flavinylated peptides were observed in the tryptic digest of CrdB and CrdA by a peptide fingerprint Mascot search.

The MS/MS analysis of the peptide with m/z of 3233.5 (Fig. S1 in the Online Resource 1) indicated that the main signals in the spectrum of fragmentation (m/z of 2794 and 2776) resulted from FMN loss in the full or dehydrated form, respectively, depending on which of the two covalent bonds, C–O or O–P, connecting the FMN moiety to the serine residue is broken. Greater intensity of the signal with m/z of 2776 indicated that the former bond is broken with greater propensity, resulting in serine dehydration [26]. Less intense but still reliable peaks in the spectrum starting from the fragment with $m/z = 2776$ also matched a series of the y -ions generated by double breaks during the fragmentation (Fig. S1, red letters, see the Online Resource 1). Here, mass difference for the Ser257 position (69 Da) corresponded to the dehydrated serine, demonstrating that fCrdB produced in ApbE-containing cells harbors an FMN residue covalently bonded to Ser257 of the predicted flavinylation motif in the *FMN bind* domain.

The non-covalently bound flavins were extracted from Crd and separated by HPLC (Fig. 2c). Both the fCrd and aCrd preparations were found to contain non-covalently bound FAD and FMN at a ratio of approximately 1 : 2.

To determine their domain localization, we prepared the genetic constructs encoding separately two *NADH:flavin* domains of CrdA and CrdB (d1 in Fig. 1a) or the *FAD binding 2* domain of CrdB (d3 in Fig. 1a). The isolated corresponding proteins exhibited the spectra characteristic of flavoproteins (Fig. 2a). The flavins present in them were again extracted and identified by HPLC (Fig. 2c). The non-covalently bound FMN was exclusively localized in the d1 fragment (*NADH:flavin* domains) whereas FAD was found in the d3 fragment (*FAD binding 2* domain). The evident corollary is that CrdAB contains two non-covalently bound FMN molecules in the oxidoreductase *NADH:flavin* domains, one non-covalently bound FAD molecule in the *FAD binding 2* domain, and one covalently bound FMN residue in the *FMN bind* domain.

The specificity of Crd for naturally occurring α,β -unsaturated carbonic acids. The similarity of the putative substrate-binding residues in the *FAD binding 2* domains of Crd and the acrylate reductase Ard of *V. harveyi* (Fig. 1b) raised the possibility that Crd also possesses acrylate reductase activity. Indeed, the Crd preparation obtained by *crdAB-apbE* coexpression (fCrd) could reduce acrylate using reduced methyl

viologen (MV) as the electron donor, but at a much lower rate (1.3 s^{-1}) compared with that of a specific acrylate reductase (19 s^{-1} [4]). Conversely, the K_m value was much greater for fCrd (770 versus $16\text{ }\mu\text{M}$), making its catalytic efficiency k_{cat}/K_m 640 times lower ($0.0019\text{ }\mu\text{M}^{-1}\text{ s}^{-1}$) compared with the acrylate reductase ($1.2\text{ }\mu\text{M}^{-1}\text{ s}^{-1}$ [4]). fCrd exhibited low but measurable activity against fumarate but was virtually inactive with methacrylate, crotonate, and urocanate (Table 1).

In contrast, cinnamate and its hydroxy derivatives were readily reduced by fCrd (k_{cat} of $22\text{--}47\text{ s}^{-1}$) and demonstrated low K_m values of $2.2\text{--}7.1\text{ }\mu\text{M}$ (Table 1). These findings classify Crd as a cinnamate reductase that is also active with other natural α,β -unsaturated cinnamate derivatives.

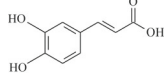
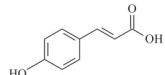
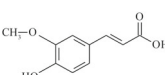
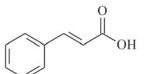
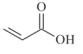
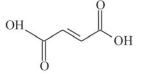
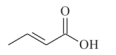
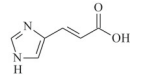
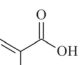
To determine the product of cinnamate reduction by fCrd, we identify it using HPLC. The Crd-catalyzed reaction was found to completely convert cinnamate to phenylpropionate (Fig. 3, a and b). The identification of the carbonic acids was supported by the observation that the peak heights on the elution profiles monitored at 210 and 258 nm were nearly equal for cinnamate but differed approximately 40-fold for phenylpropionate, in accordance with the UV-spectra of these compounds (Fig. 3c). These findings indicate that Crd reduces the α,β double bond in (hydroxy)cinnamic acids to yield their saturated derivatives. fCrd activity in the reverse reaction of phenylpropionate oxidation with phenazine methasulfate and dichlorophenolindophenol as electron acceptors was measurable but quite low (0.1 s^{-1}).

Induction of Crd synthesis in *V. ruber* cells by unsaturated carbonic acids. To determine whether the found Crd substrates induce Crd synthesis in *V. ruber*, cell growth was performed in their presence and the MV:cinnamate reductase activity was measured in cleared cell lysates. All cultivations were performed in duplicate both in the absence and in the presence of O_2 .

As Table 2 makes clear, cinnamate added at its maximal concentration (10 mM) that did not yet suppress cell growth caused appreciable induction of Crd synthesis. The effect was observed under both aerobic and anaerobic conditions but was maximal in the former case. Parallel measurements indicated a more than ten-fold increase in the gene *crdB* transcription by cinnamate, providing further support for assigning the MV:cinnamate reductase activity to Crd in *V. ruber* cells.

The other α,β -unsaturated carbonic acids acting as Crd substrates, except for acrylate, could induce Crd synthesis under anaerobic conditions (Fig. 4). These compounds were added at 2 mM concentrations because the cells did not grow anaerobically at higher concentrations of acrylate and caffeate. The effects of the carbonic acids on Crd induction thus correlated with their ability to act as substrates (Table 1).

Table 1. The reductase activity of fCrd against a series of α,β -unsaturated carbonic acids measured under anaerobic conditions with 100 μ M reduced MV as the electron donor

Substrate (acid)	Structure	k_{cat} (s^{-1})	K_m (μM)
Caffeic		47 ± 2	2.2 ± 0.4
<i>p</i> -coumaric		45 ± 3	2.4 ± 0.5
Ferulic		26 ± 2	2.8 ± 0.5
Cinnamic		22 ± 1.5	7.1 ± 0.6
Acrylic		1.3 ± 0.2	770 ± 50
Fumaric		0.20 ± 0.03^a	
Crotonic		0.06 ± 0.02^a	
Urocanic		0.04 ± 0.01^a	
Methacrylic		0.03 ± 0.01^a	

^a Value of activity measured at 1 mM substrate concentration.

Time-dependent activation of isolated Crd by NADH. The presence of the *NADH:flavin* domains in CdrAB (Fig. 1a) suggested that NADH is the natural donor of the redox equivalents for this enzyme. As ferulate, caffeate, and *p*-coumarate absorb light at 340 nm, the NADH dehydrogenase activity was tested with non-absorbing cinnamate as the electron acceptor. As the red trace in Fig. 5a highlights, the reaction initiated by cinnamate addition under anaerobic conditions demonstrated a linear NADH oxidation curve

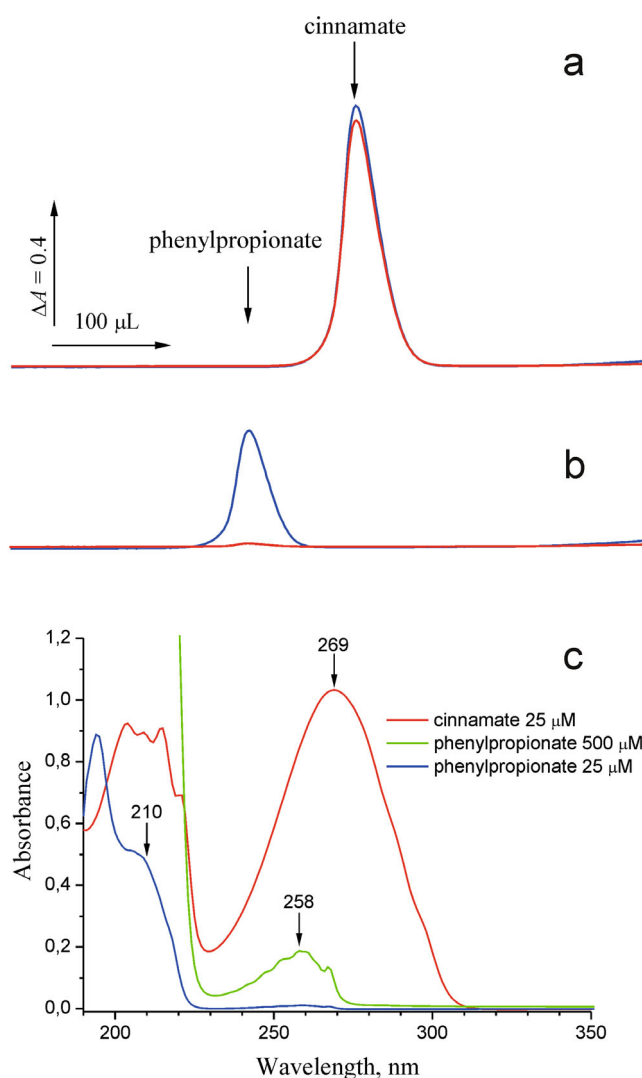


Fig. 3. HPLC identification of the product of cinnamate reduction by fCrd. Cinnamate (0.1 mM) was reacted with 10 mM sodium dithionite and 50 μM MV in the presence of 0.5 μM fCrd. a) The reaction mixture before fCrd addition. b) Same after a 30-min incubation with fCrd. The elution was monitored at 210 (blue curve) and 258 nm (red curve). The elution volumes for authentic cinnamate and phenylpropionate are indicated by arrows. c) Electronic absorption spectra of cinnamate and phenylpropionate in 10 mM potassium phosphate buffer (pH 6.5).

Table 2. Correlation between the MV:cinnamate reductase activity and *crdB* transcription level in the *V. ruber* cells cultivated in different conditions

Growth conditions	Crd activity ($\text{nmol}\cdot\text{min}^{-1}\cdot\text{mg}^{-1}$)	<i>crdB</i> mRNA/rRNA $\times 10^{-6}$
No cinnamate, no O_2	1.2 ± 0.4	2.1 ± 0.2
No cinnamate, + O_2	0.5 ± 0.2	0.8 ± 0.1
10 mM cinnamate, no O_2	86 ± 11	31 ± 4
10 mM cinnamate, + O_2	19 ± 3	25 ± 2

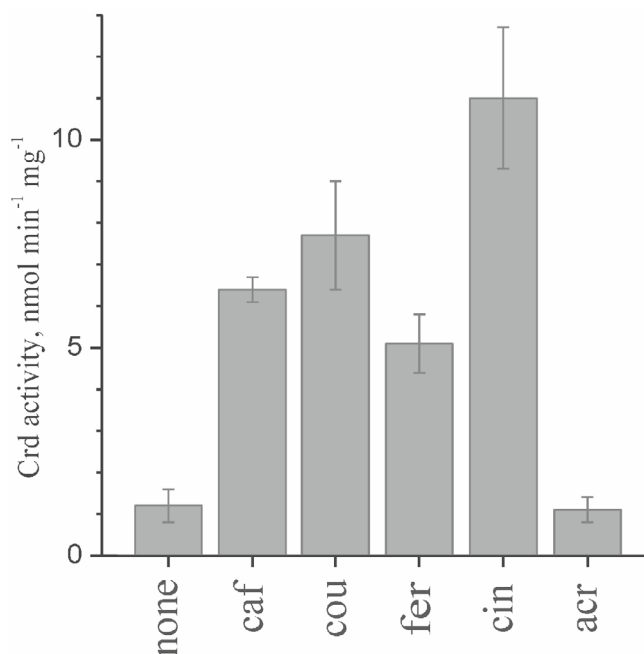


Fig. 4. MV:cinnamate reductase activity of the *V. ruber* cells grown anaerobically in the presence of 2 mM caffeine (caf), *p*-coumarate (cou), ferulate (fer), cinnamate (cin), or acrylate (acr). Error bars represent the standard deviations for two cultivations.

and a relatively high rate of 15 s⁻¹. However, changing the order of the additions affected the reaction time course dramatically. For the reaction started by fCrd, the progress curve demonstrated a profound lag in the NADH oxidation (blue trace in Fig. 5a). Although the initial slope was quite low, the final slope was similar to that for the red trace described above and likely corresponded to fully activated Crd. A similar time lag was observed in the reaction started by NADH.

These findings indicate that fCrd is inactive as isolated and requires preincubation with NADH for activation. That the length of the time lag of anaerobic cinnamate reduction started by fCrd did not depend on fCrd concentration (data not shown) indicated that the activation is not associated with changes in the oligomeric structure. Furthermore, the red trace in Fig. 5a demonstrates that the activation is much faster in the absence of cinnamate than in its presence (blue curve). The duration of Crd preincubation with NADH for the red curve in Fig. 5a was approximately 5 min and this time was thus sufficient for nearly complete activation in the absence of the electron acceptor. Preincubation with 5 mM dithionite for 5 min before starting the reaction by the enzyme activated fCrd to the same level (data not shown). These findings suggested that the activation is likely caused by the reduction of a prosthetic group in fCrd rather than by mere NADH binding to it.

For further analysis, the product formation curve for the reaction started by Crd in Fig. 5a (blue curve)

was converted into the first derivative (i.e., specific activity) plot (Fig. 5b), and its sigmoidal shape clearly indicated that the activation process is not a one-step reaction. Fitting experiments demonstrated a poor fit of the kinetic scheme involving two consecutive steps (red line) but a reasonably good fit for a scheme involving three such steps (green line). In these fittings, we assumed that the rate constants for each step are identical because this relationship corresponds to the largest possible time lag of the final product formation. The fitted value of the rate constant was 0.060 ± 0.003 s⁻¹ for the three-step reaction. Three is thus the minimal number of the steps involved in slow Crd activation by NADH.

A similar but faster activation of Crd was observed in the anaerobic acrylate reduction started by the enzyme (Fig. 5c). The maximal activity measured with this substrate (3.5 s⁻¹) was 23% of that with cinnamate. For comparison, this activity was only 1.3 s⁻¹ with MV as the electron donor (6% of the activity with cinnamate, Table 1). A similar kinetic analysis indicated that Crd activation by NADH in the presence of acrylate involves at least two steps (Fig. S2 in the Online Resource 1), both with the rate constant of 0.27 ± 0.02 s⁻¹. We also demonstrated that Crd activation by NADH in the absence of electron acceptors (Fig. S2, left panel, squares, see the Online Resource 1) was faster than in their presence (Fig. S2, left panel, circles, see the Online Resource 1; Fig. 5b, circles). A similarly kinetic analysis has revealed that the activation also involved two consecutive steps with the average rate constant of 0.75 ± 0.15 s⁻¹.

If MV was used as the electron donor with various substrates (Table 1), the progress curves were always linear irrespective of the order of fCrd and substrate additions. This result suggested that the activation/deactivation of fCrd is somehow associated with its NADH-binding *NADH:flavin* domains. This hypothesis was supported by the observation that the anaerobic NADH:FMN reduction by fCrd also demonstrated slow activation if the reaction was started by the enzyme (Fig. 5d). The activation kinetics was more complex in this case and demonstrated a poor fit of the consecutive three-step model (Fig. S2, right panel in the Online Resource 1).

Crd activated by preincubation with NADH remained active until all NADH was consumed in the enzymatic reaction, but slowly returned to the inactive state afterwards. In the experiment illustrated in Fig. 6a, the reaction was started by adding acrylate to preactivated fCrd and proceeded linearly until NADH exhaustion. A new portion of NADH restored Crd activity to the level that depended on the time interval *t* before the second NADH addition (Fig. 6b). The time-courses became nonlinear at high *t*, indicating activation as in Fig. 5c (blue trace) to a final rate

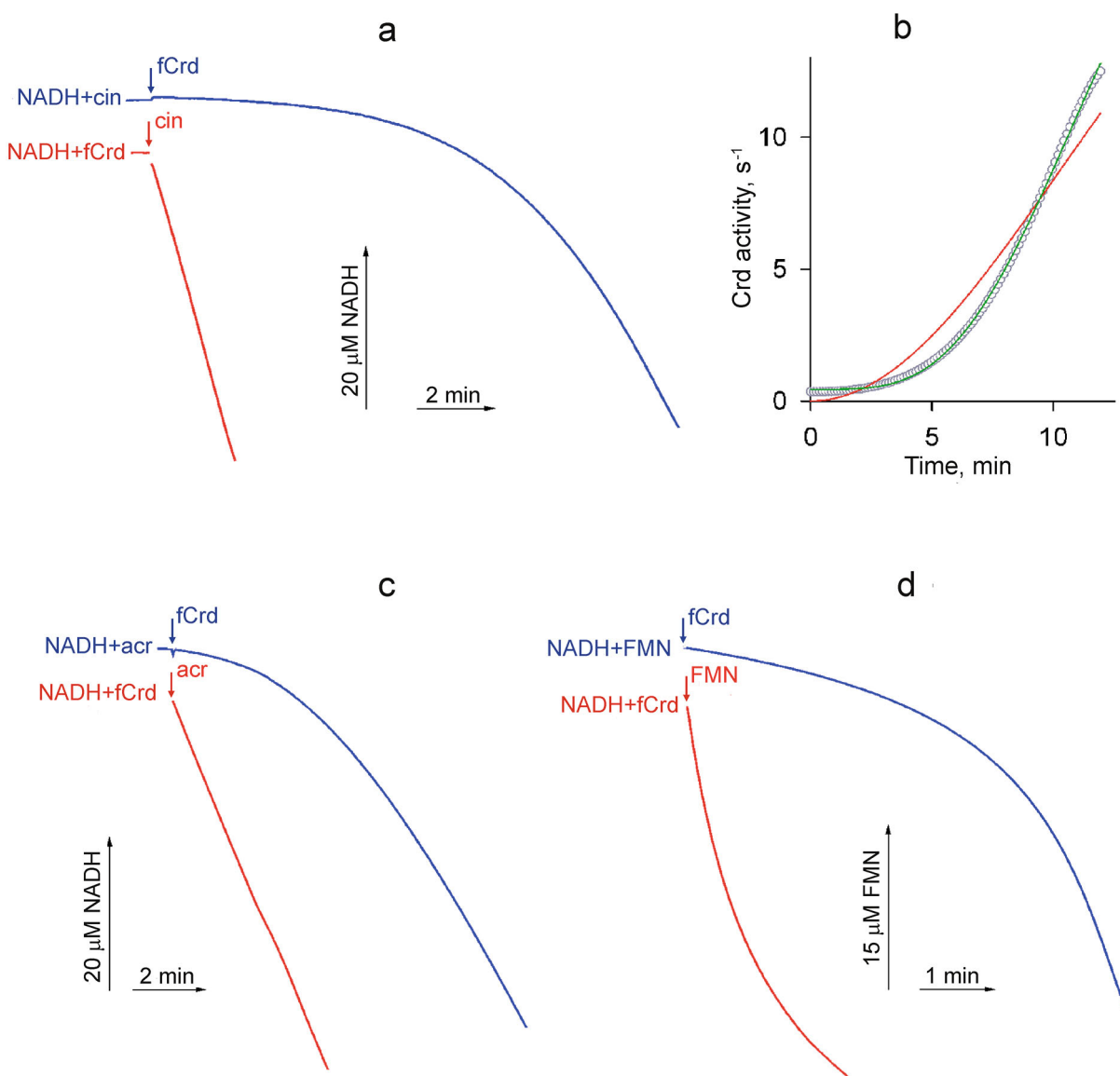


Fig. 5. The typical traces of fCrd-catalyzed NADH-dependent reactions under anaerobic conditions. a) Cinnamate-supported NADH oxidation. The final reaction mixture contained 120 μM NADH, 50 μM cinnamate, and 30 nM fCrd. The reaction was started by either cinnamate (cin, red trace) or fCrd (blue trace). b) The time dependence of Crd activity derived from the time-course of cinnamate reduction in the reaction started by Crd addition (blue curve on panel a). Small circles show the activity values determined as the slope of the tangent ($-d[\text{NADH}]/dt$) using Matlab (The Mathworks, Inc.) at 100 time points. The red and green lines show the best fits for two- and three-step kinetic models, respectively. c) Acrylate-supported NADH oxidation. The final reaction medium contained 120 μM NADH, 1 mM acrylate, and 150 nM fCrd. The reaction was started by acrylate (acr, red trace) or fCrd (blue trace). d) NADH-supported FMN reduction. The final reaction medium contained 120 μM NADH and 50 μM FMN. The fCrd concentration was 15 nM (red trace, reaction started by FMN) or 60 nM (blue trace, reaction started by fCrd).

similar to those in Fig. 5c (red trace) and 6a (left trace). These findings indicate that active fCrd is gradually deactivated when depleted of NADH but time-dependently restores full activity after NADH addition. fCrd deactivation was a first-order reaction with a half-time of 4.7 min (Fig. 6b).

Under aerobic conditions, the NADH-oxidizing activity of Crd was extremely low and did not increase with time (Fig. 7, black (1) trace). This means that oxygen prevents Crd conversion from inactive to active

state. This observation contrasts the data reported for other NADH:2-enoate and NADH:flavin reductases, which readily oxidize NADH with O_2 as the main electron acceptor [3, 4, 27]. To determine oxygen effect on active Crd, the enzyme was preincubated with NADH and allowed to convert excess cinnamate under anaerobic conditions before oxygen was added in the form of H_2O_2 (Fig. 7, red (2) trace). In this experiment, lower concentration of glucose oxidase and higher concentration of catalase were used to maintain oxygen level

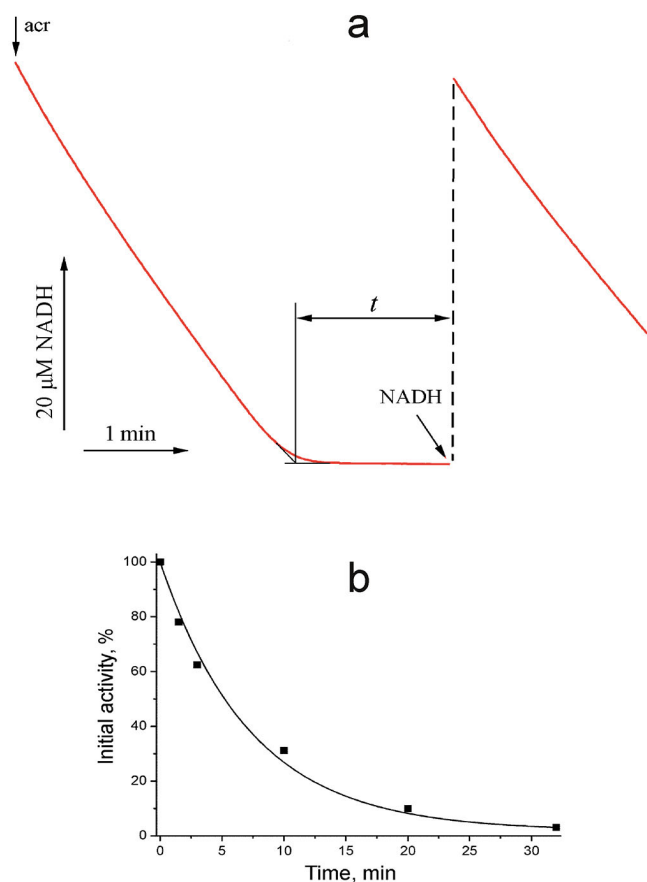


Fig. 6. Deactivation of Crd. a) Anaerobic NADH oxidation by fCrd in the presence of 1 mM acrylate (acr). When the reaction ended because of NADH consumption, its concentration was restored to the initial level ($\sim 50 \mu\text{M}$) after a 1.5-min pause. Conditions were as for Fig. 5c. b) The initial activity of NADH conversion measured for the second portion of NADH as a function of the time interval t before its re-addition. 100% refers to the initial activity estimated from the left curve in panel (a). The theoretical curve is for the first-order reaction with a half-time of 4.7 min.

in the incubation mix. As Fig. 7 highlights, the oxygen pulse caused slow inactivation of Crd, followed by slow reactivation to the initial level upon oxygen depletion by glucose oxidase. The duration of the transient inactivation phase decreased with increasing glucose oxidase concentration (data not shown). These findings indicated that the reaction of molecular oxygen with Crd, responsible for its inactivation, is easily reversible, allowing regulation of Crd activity by medium oxygen level.

Interestingly, NADPH demonstrated only low efficiency as an electron donor compared with NADH. In the corresponding experiment, fCrd preactivated by incubation with $30 \mu\text{M}$ NADH was allowed to convert acrylate until all NADH was consumed and immediately supplemented with $120 \mu\text{M}$ NADPH. The measured rate of NADPH oxidation was 35 times lower than the rate of NADH oxidation. This makes NADH the most likely physiological donor of the reducing equivalents for Crd.

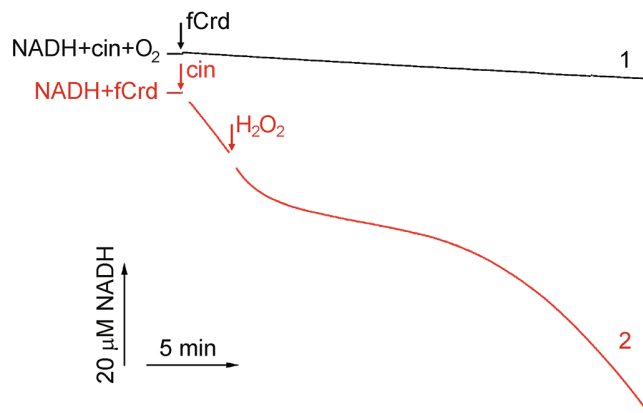


Fig. 7. Transient inactivation of Crd by oxygen pulse during NADH-supported cinnamate reduction. Trace 1) The reaction started by fCrd and carried out under aerobic conditions (no glucose oxidase and catalase added). The experimental conditions were otherwise as for the red curve in Fig. 5a. Trace 2) The reaction was started by $500 \mu\text{M}$ cinnamate and carried out under anaerobic conditions until $500 \mu\text{M}$ H_2O_2 (producing $250 \mu\text{M}$ molecular oxygen), were added at the indicated time. The concentrations of glucose oxidase and catalase in this particular experiment were 0.6 and 50 U/ml, respectively. The final reaction mixture contained $120 \mu\text{M}$ NADH and 30 nM fCrd in both experiments.

Domain roles in the catalytic activities of Crd.

Crd is thus capable of catalyzing redox reactions between different natural and artificial donors and acceptors of electrons. To determine which Crd domains are responsible for different reactions, we measured the activities of the apo- and flavinylated forms of Crd and its deletion variants. The MV:cinnamate reductase activity was high with fCrd and much lower with aCrd (no covalently bound FMN) and d3 (only *FAD binding 2* domain) (Table 3). These data indicated that, like in *Klebsiella pneumoniae* NADH:fumarate reductase [3], the *FAD binding 2* domain is required for reduction of natural electron acceptor and the electron pathway from MV to this domain involves the covalently bound FMN of the *FMN bind* domain.

In contrast, high NADH:FMN reductase activity was demonstrated not only by the full-size flavinylated enzyme (fCrd) but also by its apo-form and the d1 variant (only *NADH:flavin* domains). This reaction is thus clearly catalyzed by the *NADH:flavin* domains. Noteworthy, all the NADH:FMN reductase activities, including that manifested by the d1 variant, developed slowly in time when the reaction was started by NADH but instantly when FMN was the last added component, as in Fig. 5d.

Full NADH:cinnamate reductase activity was manifested by fCrd but not aCrd that lacks covalently bound FMN. These findings emphasized the role of the covalently bound FMN in electron transfer between the NADH dehydrogenase part (d1) and the cinnamate reductase part (d3) in Crd.

Table 3. The catalytic activities of Crd and its deletion variants^a

Enzyme/variant	Bound prosthetic groups	Activity, s ⁻¹		
		MV:cinnamate	NADH:cinnamate	NADH:FMN
fCrd	2 FMN, 1 FAD, 1 *FMN ^b	22 ± 2	15 ± 2	62 ± 15
aCrd	2 FMN, 1 FAD	0.7 ± 0.1	<0.05	58 ± 13
d1	2 FMN	n.d. ^c	<0.05	48 ± 21
d3	1 FAD	0.7 ± 0.1	<0.05	n.d.

^a The assay mixture contained 120 μM NADH or 100 μM reduced MV as the electron donor and 50 μM cinnamate or FMN as the electron acceptor. The activity values shown are for the reactions started by electron acceptor (the reactions started by the enzyme demonstrated a profound time lag).

^b The asterisk indicates covalently bound flavin.

^c n.d., not determined.

The separate *FAD binding 2* domain (d3 variant) demonstrated measurable activity ($0.60 \pm 0.05 \text{ s}^{-1}$, data not shown) in FMNH₂:cinnamate reduction, raising the possibility of catalyzing complete NADH:cinnamate reductase reaction by a 1 : 1 mixture of d1 and d3 in the presence of medium FMN. Such activity was indeed detected, and although its value, $3.2 \pm 0.4 \text{ s}^{-1}$ (data not shown), was less than for fCrd, it significantly exceeded the FMNH₂:cinnamate reductase activity of d3. This seemingly unexpected result could be, however, explained by different conditions used for the two reactions. The assay medium for the FMNH₂:cinnamate reductase activity contained, beside reduced FMN, considerable amounts of its oxidized form, which could inhibit the reaction by increasing the redox potential of the FMNH₂^{free}/FMN^{free} pair. In contrast, virtually all FMN was in the reduced form under steady-state conditions in the NADH:cinnamate reductase reaction catalyzed by d1+d3. By demonstrating full NADH:cinnamate reductase activity in the presence of medium FMN, the d1 and d3 mixture resembles yeast soluble fumarate reductase [28]. In the latter enzyme, the roles of d1 and d3 are played by separate enzymes, with free cytoplasmic flavins acting as electron carriers between them.

The modelled three-dimensional structure of Crd. The 3D structure of heterodimeric Crd was predicted using AlphaFold2 [21]. It can be divided into two parts connected by a flexible linker (Fig. 8). One of them, corresponding to the d1 fragment, is formed by CrdA and the homologous N-terminal *NADH:flavin* domain of CrdB and resembles homodimeric NADH:flavin reductases [16, 29]. The other part contains two other CrdB domains – *FAD binding 2* and *FMN bind*.

Four flavin groups (three FMNs and one FAD in their oxidized states) and one each of NADH and cinnamate molecules were docked into the modeled structure using AutoDock Vina [23]. The locations of the docked flavin groups (Fig. 8) were similar to those in

the experimentally determined structures of NAD(P)H:FMN reductase (PDB ID: 1X77 [29]), the NqrC subunit of Na⁺-translocating NADH:quinone oxidoreductase (PDB ID: 4XA7 [30]), and urocanate reductase (PDB ID: 6T87 [31]). These three proteins are homologous to the *NADH:flavin*, *FMN bind*, and *FAD binding 2* domains of Crd, respectively.

The d1 part of Crd contains two potential pseudo-symmetrical NADH-binding sites near FMN_A and FMN_B, similar to those found in the homodimeric NADH:flavin reductase [16]. However, only the FMN_B-adjacent site could be occupied by NADH because the entrance to the FMN_A-adjacent site is blocked by the C-terminal segment of CrdA (Fig. S3 in the Online Resource 1). Instead, the positions of the docked NADH molecule concentrated in two areas of the protein near FMN_A. The shortest distance between NADH and FMN_A, 10 Å, is too long for the hydride ion transfer between them (for comparison, the distance between NADH and FMN_B is only 4 Å). Similar docking experiments provided no evidence for a competent NADH-binding site in the middle, *FMN bind* domain of CrdB. The location of docked cinnamate in the *FAD binding 2* domain of CrdB was similar to that of urocanate in urocanate reductase [31].

The edge-to-edge distance between FAD and *FMN in the resulting model is approximately 9 Å (Fig. 8), allowing rapid electron transfer between these flavin groups, consistent with the finding that this step is not rate-limiting in NADH:2-enoate reductases [3]. In contrast, the FMN_B and *FMN groups are separated by 24 Å in the model (Fig. 8), a distance at which rapid electron transfer is not feasible. Clearly, Crd should adopt a different conformation to make the FMN_B and *FMN groups closer to each other and allow electron transfer between them in the catalytic reaction. Interestingly, the same step is rate-limiting in the electron transfer in canonical NADH:2-enoate reductases [3],

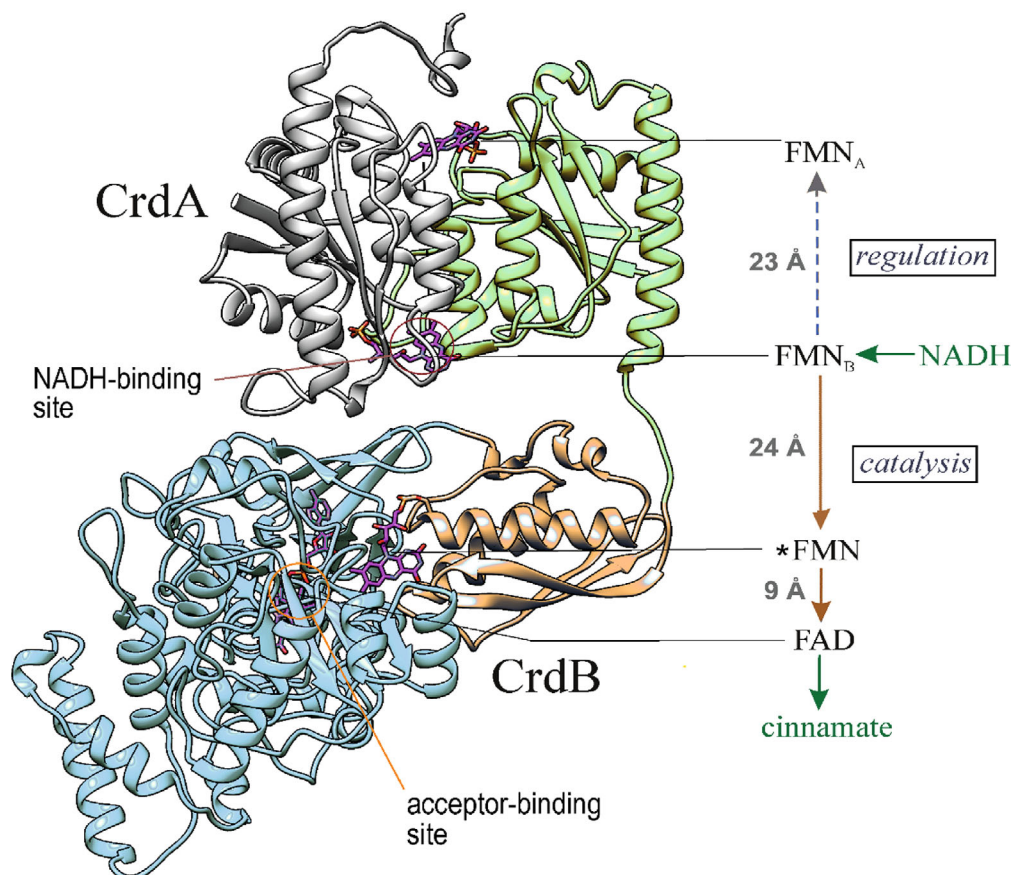


Fig. 8. The predicted three-dimensional structure of Crd with bound FAD and three FMNs in a cartoon representation. The domains are colored as in Fig. 1a. The right part shows schematically the edge-to-edge distances between the prosthetic groups and the proposed pathways for electron and hydride ion transfer (indicated by brown and green arrows, respectively).

indicating that the above distance is similarly non-optimal in these enzymes.

The validity of the model predicted by AlphaFold2 with the docked flavins was confirmed by MD simulations (Fig. S4 in the Online Resource 1). Specifically, none of the four flavin groups was lost during the simulations. Furthermore, the simulations did not change significantly the structure predicted by AlphaFold2, except for a rigid-body movement of the d1 part, connected by a flexible linker, by approximately 11 Å relative the rest of the molecule (Fig. S4, A and C in the Online Resource 1). This result showed that Crd structure is indeed flexible. However, the flavin-to-flavin distances were not appreciably different in the simulated structure (Fig. S4B in the Online Resource 1) and remained virtually unchanged in the analogous structure with the flavins in their reduced forms (data not shown).

DISCUSSION

Three-domain NADH:2-enoate reductases are abundant among anaerobic and facultatively anaerobic

prokaryotic and eukaryotic microorganisms, which suggests their metabolic importance. The enzymes with NADH:fumarate reductase activity participate in anaerobic respiration, allowing reoxidation of glycolysis-produced NADH to increase ATP production during fermentation. This role was best demonstrated in unicellular eukaryotes of the class Kinetoplastida, in which fermentation yields succinate as a major product and glycosomal and mitochondrial NADH:fumarate reductase inactivation blocks completely fumarate respiration [32]. NADH:2-enoate reductases with different substrate specificities may have other roles. Thus, NADH:acrylate reductase from marine bacterium *V. harveyi* is apparently involved in detoxication of acrylate [4], massively formed in marine habitats during degradation of dimethylsulfoniopropionate, the main compatible solute in alga.

While sharing overall structural similarity with other microbial three-domain NADH:2-enoate reductases, such as the fumarate reductases of *K. pneumoniae* and Kinetoplastida and acrylate reductase of *V. harveyi*, the *V. ruber* cinnamate reductase Crd displays significant differences. In all these enzymes, 2-enoate is reduced in *FAD binding2* domain by the electrons

transmitted via a covalently bound FMN residue of *FMN bind* domain [3]. However, the NADH-oxidizing activity belongs to *NADH:flavin* domain in Crd but to either *OYE-like* domain (in *K. pneumoniae* NADH:fumarate and *V. harveyi* NADH:acrylate reductases) or *FAD binding 6* domain (in Kinetoplastida NADH:fumarate reductases).

Furthermore, only Crd contains an additional subunit (CrdA) formed by a single *NADH:flavin* domain, which is homologous to the analogous domain of CrdB (51% identity, 65% similarity). Its gene (*crdA*) flanks the *crdB* gene in one chromosome (Fig. 1c), which, together with the finding that the tag-less CrdA co-purifies with 6×His-tagged CrdB on a Ni-column, provides strong evidence that Crd functions as a tight CrdA/CrdB complex *in vivo*. The observed noncovalently bound FMN:FAD stoichiometry of 2 : 1 is fully consistent with the heterodimeric structure of Crd. Noteworthy, prokaryotic NADH:flavin reductases are generally encoded by single genes but function as homodimers containing two bound FMN molecules at the dimer interface [16, 29]. The homodimeric structure apparently prevents direct fusion of the NADH:flavin reductase domain with other functional domains to form an extended multidomain polypeptide.

Under aerobic conditions, three-domain NADH:2-enoate reductases catalyze O₂ reduction to form reactive oxygen species (ROS). As a striking example, *K. pneumoniae* NADH:fumarate reductase oxidizes NADH to form H₂O₂ under aerobic conditions, and the oxidation reaction is not accelerated by fumarate, indicating that all NADH reducing equivalents are consumed in H₂O₂ production [3]. On the other hand, ROS production may be beneficial in some cases. Thus, ROS generation by NADH:fumarate reductases in Kinetoplastida may aid in completing the parasitic cycle (differentiation of procyclics into epimastigotes) in the insect vector [33]. However, excessive ROS generation upon transfer to aerobiosis is expected to be harmful for most facultatively anaerobic microorganisms. For instance, accumulation of H₂O₂ in millimolar concentrations under the action of NADH:flavin reductase in aerobic conditions caused cell death in the lactic acid bacterium *Lactobacillus johnsonii* [27].

The presence of a pair of *NADH:flavin* domains in *V. ruber* Crd instead of the *OYE-like* or *FAD binding 6* domain found in other NADH:2-enoate reductases presumably solves the problem of excessive ROS production. The *NADH:flavin* domains allow a unique regulation mechanism that reversibly blocks Crd activity at high O₂ concentrations (Fig. 7). The transition between the active and inactive states appears to be controlled in Crd by the redox state of one or both FMN molecules in the *NADH:flavin* domains. This conclusion is supported by the observations that Crd could be activated by both NADH and dithionite and that the d1 but

not d3 fragment demonstrated similar time-dependent activation of its partial enzymatic activity.

Crd regulation appears to be associated with the heterodimeric structure of the NADH dehydrogenase part, formed by CrdA and the homologous N-terminal domain of CrdB (Fig. 8). This part of Crd resembles NADH:flavin reductases [16, 29] and similarly contains two noncovalently bound FMN groups and two potential sites of NADH oxidation. However, the competence of the putative NADH-binding site near FMN_A seems questionable because of the unfavorable steric effect of the C-terminal loop of CrdA. While electron transfer between FMN_B and *FMN is perceivable assuming *FMN and/or *NADH:flavin* dimer flexibility, the long distance between FMN_B and FMN_A (Fig. 8) can hardly decrease similarly. Hence, the electron transfer between these flavin groups should be always much slower than enzyme turnover [34]. These structural considerations suggest that FMN_B and FMN_A are good candidates for the catalytic and regulating groups, respectively. That these flavins have distinct roles is consistent with significant differences in the amino acid sequences of the two *NADH:flavin* domains of Crd, contrasting the case of homodimeric and, hence, symmetrical NADH:flavin reductases in which two FMN sites are identical [16]. One can further speculate that Crd activation involves the stepwise reduction of FMN_B and FMN_A causing a conformational change that forms a functional electron transfer chain linking the donor and acceptor.

That the electron acceptors slow down Crd activation by NADH raises the possibility that the bound acceptor competes with the regulating prosthetic group, likely FMN_A, for the electrons coming from NADH. In this case, the activation rate should inversely correlate with the rate of acceptor reduction. Such a correlation was indeed observed – cinnamate was reduced faster (Table 1) and decelerated Crd activation more compared with acrylate (Fig. 5). In this context, the lack of Crd activation under aerobic conditions may mean that O₂ can oxidize the regulating prosthetic group directly, without using the long electron transfer chain involved in the case of cinnamate and acrylate.

Despite the similarity of the 2-enoate-binding amino acid residues in the *FAD binding 2* domains of acrylate reductase and Crd (Fig. 1b), the latter enzyme exhibits a 1000-6000-fold lower catalytic efficiency against acrylate than against cinnamate and its derivatives (Table 1). Furthermore, (hydroxy)cinnamic acids, but not acrylate, induced Crd synthesis in *V. ruber* cells (Fig. 4). Clearly, the positions of amino acid residues interacting with electron-acceptor carboxylates in fumarate reductases are not the only determinants of the substrate specificity in other NADH:2-enoate reductases. The reduction of cinnamate and its derivatives, toxic to cells [35], is thus the most likely physio-

logical function of Crd, and this inference is supported by their induction of Crd synthesis in both anaerobic and aerobic conditions (Table 2). Additionally, Crd may support anaerobic respiration of *V. ruber* on (hydroxy) cinnamic acids as described for caffeoyl-CoA reductase from acetogenic bacterium *Acetobacterium woodii* [36]. The most effective substrates of Crd, caffeate and ferulate, are the precursors of lignin and various phenolic secondary metabolites in plants. That is why these compounds are abundant in terrestrial niches, soil, and animal gut in particular, but are relatively rare in the marine habitats, where they are synthesized in some algae [37, 38]. An interesting exception to this rule is the seagrass meadows, which accumulate caffeic acid and other phenolic compounds in rhizosphere [35], a likely main habitat for Crd-containing marine bacteria [39].

Crd-like reductases are relatively rare among marine microorganisms, seemingly, because (hydroxyl) cinnamic acids are underrepresented in the habitat. BLAST search has revealed Crd-like proteins only in the following marine bacteria: *Vibrio rhizosphaerae*, *Vibrio gazogenes*, *Vibrio salinus*, *Vibrio spartinae*, and *Vibrio tritonius*. However, such reductases are abundant among anaerobic and facultatively anaerobic terrestrial bacteria (the *Clostridium*, *Klebsiella*, *Citrobacter*, *Aeromonas*, *Paenibacillus*, *Streptococcus*, and other genera), including those forming human intestinal microbiome. The presence of substantial amounts of phenylpropionate and *p*-hydroxyphenylpropionate in the mammalian intestine has long been known [40] but their production was attributed to a different enzyme, bacterial two-domain 2-enoate reductase [1]. The wide distribution of Crd-like enzymes among intestinal bacteria suggests that they are also involved in phenylpropionate and *p*-hydroxyphenylpropionate formation in the mammalian intestine.

Two-domain 2-enoate reductases are industrial biocatalysts increasingly used to produce chiral intermediates, pharmaceuticals and agrochemicals [11, 41]. A disadvantage of these enzymes is that they are readily and irreversibly inactivated by oxygen [1, 11]. The lower sensitivity of Crd to oxygen makes it a promising alternative for industrial application.

Contributions. AVB the conception of the study; YVB, MVS, VAA, AAB, and AVB the acquisition and analysis of the data; AAB and AVB writing of the manuscript.

Acknowledgments. MALDI MS and laser scanner facilities became available to us in the framework of the Moscow State University Development Program PNG 5.13. This article is devoted to cherished memory of Vladimir P. Skulachev.

Funding. This work was supported by the Russian Science Foundation (project no. 22-24-00133).

Ethics declarations. The authors declare no conflicts of interest. This article does not contain description of studies with the involvement of humans or animal subjects.

Electronic supplementary material. The online version contains supplementary material available at <https://doi.org/10.1134/S0006297924020056>.

REFERENCES

1. Tischer, W., Bader, J., and Simon, H. (1979) Purification and some properties of a hitherto-unknown enzyme reducing the carbon-carbon double bond of α,β -unsaturated carboxylate anions, *Eur. J. Biochem.*, **97**, 103-112, doi: 10.1111/j.1432-1033.
2. Besteiro, S., Biran, M., Biteau, N., Coustou, V., Baltz, T., Canioni, P., and Bringaud, F. (2002) Succinate secreted by *Trypanosoma brucei* is produced by a novel and unique glycosomal enzyme, NADH-dependent fumarate reductase, *J. Biol. Chem.*, **277**, 38001-38012, doi: 10.1074/jbc.M201759200.
3. Bertsova, Y. V., Oleynikov, I. P., and Bogachev, A. V. (2020) A new water-soluble bacterial NADH: fumarate oxidoreductase, *FEMS Microbiol. Lett.*, **367**, fnaa175, doi: 10.1093/femsle/fnaa175.
4. Bertsova, Y. V., Serebryakova, M. V., Baykov, A. A., and Bogachev, A. V. (2022) A novel, NADH-dependent acrylate reductase in *Vibrio harveyi*, *Appl. Environ. Microbiol.*, **88**, e0051922, doi: 10.1128/aem.00519-22.
5. Bertsova, Y. V., Kostyrko, V. A., Baykov, A. A., and Bogachev, A. V. (2014) Localization-controlled specificity of FAD:threonine flavin transferases in *Klebsiella pneumoniae* and its implications for the mechanism of Na⁺-translocating NADH:quinone oxidoreductase, *Biochim. Biophys. Acta*, **1837**, 1122-1129, doi: 10.1016/j.bbabi.2013.12.006.
6. Serebryakova, M. V., Bertsova, Y. V., Sokolov, S. S., Kolesnikov, A. A., Baykov, A. A., and Bogachev, A. V. (2018) Catalytically important flavin linked through a phosphoester bond in a eukaryotic fumarate reductase, *Biochimie*, **149**, 34-40, doi: 10.1016/j.biochi.2018.03.013.
7. Rohdich, F., Wiese, A., Feicht, R., Simon, H., and Bacher, A. (2001) Enoate reductases of *Clostridia*. Cloning, sequencing, and expression, *J. Biol. Chem.*, **276**, 5779-5787, doi: 10.1074/jbc.M008656200.
8. Kuno, S., Bacher, A., and Simon, H. (1985) Structure of enoate reductase from a *Clostridium tyrobutyricum* (*C. spec.* La1), *Biol. Chem. Hoppe Seyler*, **366**, 463-472, doi: 10.1515/bchm3.1985.366.1.463.
9. Caldeira, J., Feicht, R., White, H., Teixeira, M., Moura, J. J., Simon, H., and Moura, I. (1996) EPR and Mössbauer spectroscopic studies on enoate reductase, *J. Biol. Chem.*, **271**, 18743-18748, doi: 10.1074/jbc.271.31.18743.
10. Giesel, H., and Simon, H. (1983) On the occurrence of enoate reductase and 2-oxo-carboxylate reductase in

- clostridia and some observations on the amino acid fermentation by *Peptostreptococcus anaerobius*, *Arch. Microbiol.*, **135**, 51-57, doi: 10.1007/BF00419482.
11. Mordaka, P. M., Hall, S. J., Minton, N., and Stephens, G. (2018) Recombinant expression and characterisation of the oxygen-sensitive 2-enoate reductase from *Clostridium sporogenes*, *Microbiology (Reading)*, **164**, 122-132, doi: 10.1099/mic.0.000568.
 12. Shieh, W. Y., Chen, Y. W., Chaw, S. M., and Chiu, H. H. (2003) *Vibrio ruber* sp. nov., a red, facultatively anaerobic, marine bacterium isolated from sea water, *Int. J. Syst. Evol. Microbiol.*, **53**, 479-484, doi: 10.1099/ijs.0.02307-0.
 13. Bogachev, A. V., Bertsova, Y. V., Bloch, D. A., and Verkhovskiy, M. I. (2012) Urocanate reductase: Identification of a novel anaerobic respiratory pathway in *Shewanella oneidensis* MR-1, *Mol. Microbiol.*, **86**, 1452-1463, doi: 10.1111/mmi.12067.
 14. Light, S. H., Méheust, R., Ferrell, J. L., Cho, J., Deng, D., Agostoni, M., Iavarone, A. T., Banfield, J. F., D'Orazio, S. E. F., and Portnoy, D. A. (2019) Extracellular electron transfer powers flavinylated extracellular reductases in Gram-positive bacteria, *Proc. Natl. Acad. Sci. USA*, **116**, 26892-26899, doi: 10.1073/pnas.1915678116.
 15. Bogachev, A. V., Baykov, A. A., and Bertsova, Y. V. (2018) Flavin transferase: the maturation factor of flavin-containing oxidoreductases, *Biochem. Soc. Trans.*, **46**, 1161-1169, doi: 10.1042/BST20180524.
 16. Koike, H., Sasaki, H., Kobori, T., Zenno, S., Saigo, K., Murphy, M. E., Adman, E. T., and Tanokura, M. (1998) 1.8 Å crystal structure of the major NAD(P)H:FMN oxidoreductase of a bioluminescent bacterium, *Vibrio fischeri*: overall structure, cofactor and substrate-analog binding, and comparison with related flavoproteins, *J. Mol. Biol.*, **280**, 259-273, doi: 10.1006/jmbi.1998.1871.
 17. Bertsova, Y. V., Kulik, L. V., Mamedov, M. D., Baykov, A. A., and Bogachev, A. V. (2019) Flavodoxin with an air-stable flavin semiquinone in a green sulfur bacterium, *Photosynth. Res.*, **142**, 127-136, doi: 10.1007/s11120-019-00658-1.
 18. Bertsova, Y. V., Fadeeva, M. S., Kostyrko, V. A., Serebryakova, M. V., Baykov, A. A., and Bogachev, A. V. (2013) Alternative pyrimidine biosynthesis protein ApbE is a flavin transferase catalyzing covalent attachment of FMN to a threonine residue in bacterial flavoproteins, *J. Biol. Chem.*, **288**, 14276-14286, doi: 10.1074/jbc.M113.455402.
 19. Laemmli, U. K. (1970) Cleavage of structural proteins during the assembly of the head of bacteriophage T4, *Nature*, **227**, 680-685, doi: 10.1038/227680a0.
 20. Ells, A. H. (1959) A colorimetric method for the assay of soluble succinic dehydrogenase and pyridinenucleotide-linked dehydrogenases, *Arch. Biochem. Biophys.*, **85**, 561-562, doi: 10.1016/0003-9861(59)90527-2.
 21. Jumper, J., Evans, R., Pritzel, A., Green, T., Figurnov, M., Ronneberger, O., Tunyasuvunakool, K., Bates, R., Židek, A., Potapenko, A., Bridgland, A., Meyer, C., Kohl, S. A. A., Ballard, A. J., Cowie, A., Romera-Paredes, B., Nikolov, S., Jain, R., Adler, J., Back, T., Petersen, S., Reiman, D., Clancy, E., Zielinski, M., Steinegger, M., Pacholska, M., Berghammer, T., Bodenstein, S., Silver, D., Vinyals, O., Senior, A. W., Kavukcuoglu, K., Kohli, P., and Hassabis, D. (2021) Highly accurate protein structure prediction with AlphaFold, *Nature*, **596**, 583-589, doi: 10.1038/s41586-021-03819-2.
 22. Mirdita, M., Schütze, K., Moriawaki, Y., Heo, L., Ovchinnikov, S., and Steinegger, M. (2022) ColabFold: making protein folding accessible to all, *Nat. Meth.*, **19**, 679-682, doi: 10.1038/s41592-022-01488-1.
 23. Trott, O., and Olson, A. J. (2010) AutoDock Vina: improving the speed and accuracy of docking with a new scoring function, efficient optimization, and multithreading, *J. Comput. Chem.*, **31**, 455-461, doi: 10.1002/jcc.21334.
 24. Case, D.A., Aktulga, H. M., Belfon, K., Ben-Shalom, I. Y., Berryman, J. T., Brozell, S. R., et al. (2022) Amber 2022, University of California, San Francisco.
 25. Bolanos-Garcia, V. M., and Davies, O. R. (2006) Structural analysis and classification of native proteins from *E. coli* commonly co-purified by immobilised metal affinity chromatography, *Biochim. Biophys. Acta*, **1760**, 1304-1313, doi: 10.1016/j.bbagen.2006.03.027.
 26. Bertsova, Y. V., Serebryakova, M. V., Baykov, A. A., and Bogachev, A. V. (2021) The flavin transferase ApbE flavinylates the ferredoxin:NAD⁺-oxidoreductase Rnf required for N₂ fixation in *Azotobacter vinelandii*, *FEMS Microbiol. Lett.*, **368**, fnab130, doi: 10.1093/femsle/fnab130.
 27. Hertzberger, R., Arents, J., Dekker, H. L., Pridmore, R. D., Gysler, C., Kleerebezem, M., and de Mattos, M. J. (2014) H₂O₂ production in species of the *Lactobacillus acidophilus* group: a central role for a novel NADH-dependent flavin reductase, *Appl. Environ. Microbiol.*, **80**, 2229-2239, doi: 10.1128/AEM.04272213.
 28. Kim, S., Kim, C. M., Son, Y. J., Choi, J. Y., Siegenthaler, R. K., Lee, Y., Jang, T. H., Song, J., Kang, H., Kaiser, C. A., and Park, H. H. (2018) Molecular basis of maintaining an oxidizing environment under anaerobiosis by soluble fumarate reductase, *Nat. Commun.*, **9**, 4867, doi: 10.1038/s41467-018-07285-9.
 29. Agarwal, R., Bonanno, J. B., Burley, S. K., and Swaminathan, S. (2006) Structure determination of an FMN reductase from *Pseudomonas aeruginosa* PA01 using sulfur anomalous signal, *Acta Crystallogr. D Biol. Crystallogr.*, **62**, 383-391, doi: 10.1107/S09074444906001600.
 30. Borshchevskiy, V., Round, E., Bertsova, Y., Polovinkin, V., Gushchin, I., Ishchenko, A., Kovalev, K., Mishin, A., Kachalova, G., Popov, A., Bogachev, A., and Gordeliy, V. (2015) Structural and functional investigation of flavin binding center of the NqrC subunit of sodium-translocating NADH:quinone oxidore-

- ductase from *Vibrio harveyi*, *PLoS One*, **10**, e0118548, doi: 10.1371/journal.pone.0118548.
31. Venskutonytė, R., Koh, A., Stenström, O., Khan, M. T., Lundqvist, A., Akke, M., Bäckhed, F., and Lindkvist-Petersson, K. (2021) Structural characterization of the microbial enzyme urocanate reductase mediating imidazole propionate production, *Nat. Commun.*, **12**, 1347, doi: 10.1038/s41467-021-21548-y.
 32. Coustou, V., Besteiro, S., Rivière, L., Biran, M., Biteau, N., Franconi, J. M., Boshart, M., Baltz, T., and Bringaud, F. (2005) A mitochondrial NADH-dependent fumarate reductase involved in the production of succinate excreted by procyclic *Trypanosoma brucei*, *J. Biol. Chem.*, **280**, 16559-16570, doi: 10.1074/jbc.M500343200.
 33. Wargnies, M., Plazolles, N., Schenk, R., Villafranz, O., Dupuy, J. W., Biran, M., Bachmaier, S., Baudouin, H., Clayton, C., Boshart, M., and Bringaud, F. (2021) Metabolic selection of a homologous recombination-mediated gene loss protects *Trypanosoma brucei* from ROS production by glycosomal fumarate reductase, *J. Biol. Chem.*, **296**, 100548, doi: 10.1016/j.jbc.2021.100548.
 34. Page, C. C., Moser, C. C., Chen, X., and Dutton, P. L. (1999) Natural engineering principles of electron tunnelling in biological oxidation-reduction, *Nature*, **402**, 47-52, doi: 10.1038/46972.
 35. Sogin, E. M., Michellod, D., Gruber-Vodicka, H. R., Bourceau, P., Geier, B., Meier, D. V., Seidel, M., Ahmerkamp, S., Schorn, S., D'Angelo, G., Procaccini, G., Dubilier, N., and Liebeke, M. (2022) Sugars dominate the seagrass rhizosphere, *Nat. Ecol. Evol.*, **6**, 866-877, doi: 10.1038/s41559-022-01740-z.
 36. Bertsch, J., Parthasarathy, A., Buckel, W., and Müller, V. (2013) An electron-bifurcating caffeoyl-CoA reductase, *J. Biol. Chem.*, **288**, 11304-11311, doi: 10.1074/jbc.M112.444919.
 37. Martone, P. T., Estevez, J. M., Lu, F., Ruel, K., Denny, M. W., Somerville, C., and Ralph, J. (2009) Discovery of lignin in seaweed reveals convergent evolution of cell-wall architecture, *Curr. Biol.*, **19**, 169-175, doi: 10.1016/j.cub.2008.12.031.
 38. Fernando, I. P., Kim, M., Son, K. T., Jeong, Y., and Jeon, Y. J. (2016) Antioxidant activity of marine algal polyphenolic compounds: a mechanistic approach, *J. Med. Food*, **19**, 615-628, doi: 10.1089/jmf.2016.3706.
 39. Rameshkumar, N., and Nair, S. (2009) Isolation and molecular characterization of genetically diverse antagonistic, diazotrophic red-pigmented vibrios from different mangrove rhizospheres, *FEMS Microbiol. Ecol.*, **67**, 455-467, doi: 10.1111/j.1574-6941.2008.00638.x.
 40. Smith, E. A., and Macfarlane, G. T. (1996) Enumeration of human colonic bacteria producing phenolic and indolic compounds: effects of pH, carbohydrate availability and retention time on dissimilatory aromatic amino acid metabolism, *J. Appl. Bacteriol.*, **81**, 288-302, doi: 10.1111/j.1365-2672.1996.tb04331.x.
 41. Knaus, T., Toogood, H. S., and Scrutton, N. S. (2016) *Ene-Reductases and Their Applications. Green Biocatalysis*, John Wiley and Sons, Inc., pp. 473-488, doi: 10.1002/9781118828083.ch18.
 42. Sievers, F., and Higgins, D. G. (2018) Clustal Omega for making accurate alignments of many protein sequences, *Protein Sci.*, **27**, 135-145, doi: 10.1002/pro.3290.

Publisher's Note. Pleiades Publishing remains neutral with regard to jurisdictional claims in published maps and institutional affiliations.